A&A 607, L6 (2017)
DOI: 10.1051/0004-6361/201731691

Astronomy & Astrophysics

Letter to the Editor

ALMA discovery of a rotating SO/SO_2 flow in HH212

A possible MHD disk wind?

B. Tabone[1], S. Cabrit[1,2], E. Bianchi[3,4], J. Ferreira[2], G. Pineau des Forêts[1,5], C. Codella[3], A. Gusdorf[1], F. Gueth[6], L. Podio[3], and E. Chapillon[6,7]

[1] LERMA, Observatoire de Paris, PSL Research University, CNRS, Sorbonne Université, UPMC Univ. Paris 06, 75014 Paris, France
e-mail: benoit.tabone@obspm.fr
[2] Univ. Grenoble Alpes, CNRS, IPAG, 38000 Grenoble, France
[3] INAF, Osservatorio Astrofisico di Arceti, Largo E. Fermi 5, 50125 Firenze, Italy
[4] Università degli Studi di Firenze, Dipartimento di Fisica e Astronomia, via G. Sansone 1, 50019 Sesto Fiorentino, Italy
[5] Institut d'Astrophysique Spatiale, CNRS UMR 8617, Université Paris-Sud, 91405 Orsay, France
[6] Institut de Radioastronomie Millimétrique, 38406 Saint-Martin d'Hères, France
[7] OASU/LAB-UMR5804, CNRS, Université Bordeaux, 33615 Pessac, France

Received 1 August 2017 / Accepted 29 September 2017

ABSTRACT

We wish to constrain the possible contribution of a magnetohydrodynamic disk wind (DW) to the HH212 molecular jet. We mapped the flow base with ALMA Cycle 4 at 0.″13 ~ 60 au resolution and compared these observations with synthetic DW predictions. We identified, in SO/SO_2, a rotating flow that is wider and slower than the axial SiO jet. The broad outflow cavity seen in $C^{34}S$ is not carved by a fast wide-angle wind but by this slower agent. Rotation signatures may be fitted by a DW of a moderate lever arm launched out to ~40 au with SiO tracing dust-free streamlines from 0.05−0.3 au. Such a DW could limit the core-to-star efficiency to ≤50%.

Key words. stars: formation – ISM: jets and outflows – ISM: individual objects: HH212

1. Introduction

The question of angular momentum extraction from protoplanetary disks (hereafter PPDs) is fundamental in understanding the accretion process in young stars and the formation conditions of planets. Pioneering semi-analytical work, followed by a growing body of magnetohydrodynamic (MHD) simulations, have shown that when a significant vertical magnetic field is present, MHD disk winds (hereafter DWs) can develop that extract some or all of the angular momentum flux required for accretion (see e.g. Ferreira et al. 2006; Béthune et al. 2017; Zhu & Stone 2017, and references therein). The wind dynamics depend crucially on the disk magnetization, surface heating, and ionization structure, which are still poorly known in PPDs. Observing signatures of DWs would thus provide unique clues to these properties.

Spatially resolved rotation signatures suggestive of a DW were first reported in the intermediate velocity component ($V \simeq 50$ km s^{-1}) surrounding the DG Tau optical atomic jet by Bacciotti et al. (2002). Their variation with radius was found to be in excellent agreement with synthetic predictions for an extended DW that extracts all of the accretion angular momentum out to a radius of 3 au (Pesenti et al. 2004). The inner regions of the same DW could also explain the speed of the fast axial jet (Ferreira et al. 2006). However, rotation signatures in this faster component are less clear (e.g. Louvet et al. 2016) because of the limited spectral resolution and wavelength accuracy in the optical. Sub/mm interferometric observations do not have this limitation and have provided clear evidence for flow rotation in several younger protostellar sources, although at lower speeds than the axial jets, suggesting ejection from ~5−25 au in the disk (Launhardt et al. 2009; Matthews et al. 2010; Bjerkeli et al. 2016; Hirota et al. 2017). Thermo-chemical models show that dusty DWs launched from this range of radii would indeed remain molecular despite magnetic acceleration (Panoglou et al. 2012). These models would also reproduce all characteristics of the ubiquitous broad (±40 km s^{-1}) H_2O line components revealed by *Herschel* in low-mass protostars (Yvart et al. 2016).

More stringent tests of the DW paradigm require high angular resolution. Using ALMA observations with an 8 au beam, Lee et al. (2017a) recently detected evidence for rotation in fast SiO jet knots from the HH212 protostar in the same sense as the rotating envelope. Assuming steady magneto-centrifugal launching and taking the observed gradient as a direct measure of specific angular momentum, these authors inferred a launch radius of $0.05^{+0.05}_{-0.02}$ au, which suggested that the SiO jet arises from the inner disk edge. Here we present Cycle 4 ALMA observations of the same source at 0.″13 ~ 60 au resolution (for d = 450 pc), which reveal rotation in SO_2 and SO in the same sense as the SiO jet, but in a wider structure surrounding it. We compare the observations with synthetic predictions for extended DWs to constrain the possible range of launch radii and magnetic lever arm, and we discuss the major implications of our findings.

2. Observations

HH212 was observed in Band 7 with ALMA between 6 October and 26 November 2016 (Cycle 4) using 44 antennas of the 12 m array with a maximum baseline of 3 km. The $SO_2(8_{2,6}-7_{1,7})$ line at 334.67335 GHz was observed with a spectral resolution of 1 km s^{-1} and the lines of $SO(9_8-8_7)$ 346.52848 GHz, SiO(8−7) 347.33063 GHz, $C^{34}S$(7−6) 337.39669 GHz, and $C^{17}O$(3−2) 337.06113 GHz with a spectral resolution of 0.1 km s^{-1} (rebinned to 0.44 km s^{-1}). Calibration was carried out following

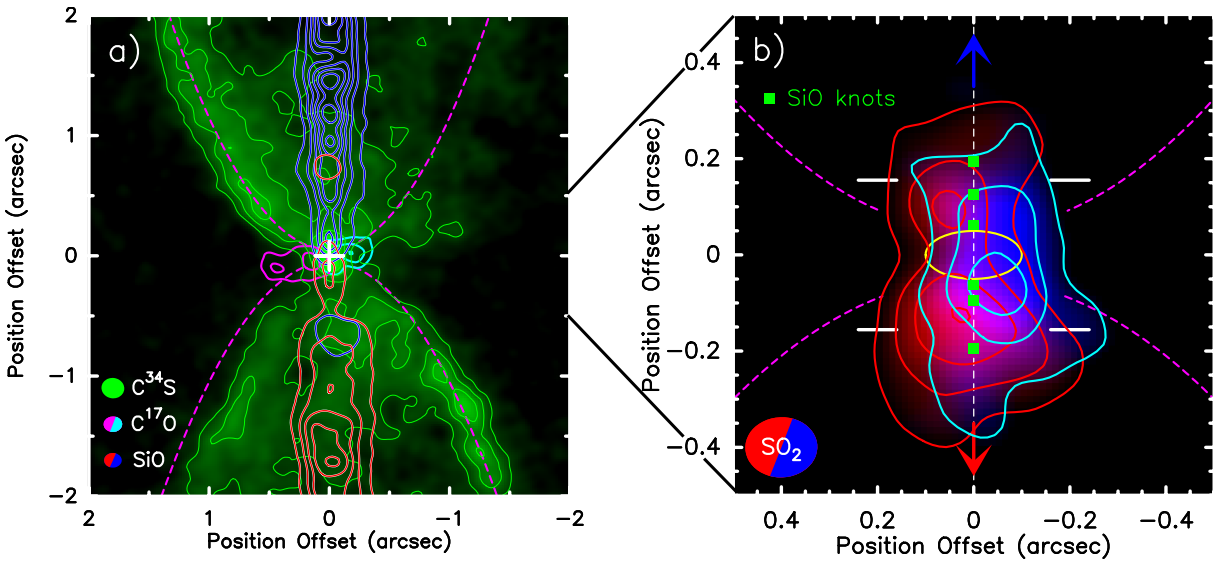

Fig. 1. *Panel a*: HH212 inner region viewed by ALMA Cycle 4. The SiO jet at $|V_{\rm LSR} - V_{\rm sys}|$= 5−10 km s^{-1} (blue and red contours), C^{17}O rotating envelope at $|V_{\rm LSR} - V_{\rm sys}|$= 1.5 km s^{-1} (pink and turquoise), and cavity walls in C^{34}S at $|V_{\rm LSR} - V_{\rm sys}|\leq$ 0.6 km s^{-1} (green, with parabolic fits in dashed magenta) are shown. First contour and step are 6σ and 18σ for SiO, 6σ and 6σ for C^{17}O, 4σ and 4σ for C^{34}S, where σ is the rms noise level. The source is shown as a white cross and beam sizes are in the bottom left corner. *Panel b*: zoom-in on blue and red SO_2 at ±2 km s^{-1} shows a slow outflow rotating in the same sense as the C^{17}O disk. First contour and step are 7σ. White segments show the positions of PV cuts in Fig 2. Green squares show inner SiO knots imaged by Lee et al. (2017a); the yellow ellipse marks the centrifugal barrier radius at $r \sim 45$ au and the height of the COM-rich disk atmosphere at $z \pm 20$ au (Lee et al. 2017c). Images are rotated such that the vertical axis corresponds to the jet axis at PA = 22°.

standard procedures under the CASA environment using quasars J0510+1800, J0552+0313, J0541−0211, and J0552−3627. Spectral line imaging was performed in CASA with natural weighting for C^{34}S to increase sensitivity, resulting in a clean-beam 0.19″ × 0.17″ (PA = −76°), and with a R = 0.5 robust factor for the other lines, resulting in a beam of .15″ × 0.13″ (PA ∼ −89°). The rms noise level is $\sigma \sim 1$ mJy/beam in SO_2 in 1 km s^{-1} channels, and $\sigma \sim 1.5$ mJy/beam in 0.44 km s^{-1} channels for the other lines. Further data analysis was performed using the GILDAS[1] package. Positions are given with respect to the continuum peak at α(J2000) = 05$^{\rm h}$ 43$^{\rm m}$ 51$^{\rm s}$.41, δ(J2000) = −01° 02′ 53″.17 (Lee et al. 2014) and velocities are with respect to a systemic velocity $V_{\rm sys}$ = 1.7 km s^{-1} (Lee et al. 2014).

3. Results and discussion

3.1. Evidence for a rotating wide-angle flow in SO and SO_2

Figure 1a presents a view of the various components of the HH 212 outflow system from our Cycle 4 data. The chemical stratification first noted by Codella et al. (2014) in Cycle 0 is even more striking: SiO traces the narrow high-velocity jet, while C^{34}S outlines the dense walls of a broad outflow cavity, and C^{17}O traces the rotating equatorial envelope and disk. We find that the cavity walls may be fitted by a parabolic shape $z = r^2/a + 0.05''$ with $a = 0.9''$ in the north and $a = 1''$ in the south (slightly less open than sketched in Lee et al. 2017c).

Figure 1b presents a zoom on SO_2 emission within 0.5″ = 250 au of the source. This tracer, together with SO, was found to be abundant in the HH 212 jet on a larger scale (Podio et al. 2015). Our data resolve its bright emission near the base, revealing a rotation signature in the form of a transverse shift ≃ ±0.05″ between redshifted and blueshifted emission at ±2 km s^{-1} from systemic, in the same (east-west) sense in both lobes and in the same sense as the envelope rotation in Fig. 1a. The emission peaks at a typical distance of 0.1−0.15″, well above the disk atmosphere at $z \simeq \pm 0.05''$ traced by complex organic molecules (Lee et al. 2017c; Bianchi et al. 2017) and extends out to ± 0.3″ along the jet axis, indicating that this rotating material is outflowing. In the equatorial plane, the emission appears to originate from a region of typical radius ≃0.1″ = 45 au, i.e., similar to the centrifugal barrier (herafter CB) estimated from HCO^+ infall kinematics, inside which the disk is expected to become Keplerian (Lee et al. 2017c). Channel maps (see Fig. A.1) further show that this rotating outflow has an onion-like velocity structure with increasing width at progressively lower velocities, which eventually fills up the base of the cavity. The SO emission has a similar behavior (see Fig. A.2). Figure 2 shows transverse position-velocity (PV) cuts and line profiles of SO_2 and SO at ±70 au from the midplane (beyond 1 beam diameter, to avoid any contamination by infall). Rotation is clearly apparent as a tilt in the PV cuts. The velocity decrease away from the jet axis is also visible. The centroid velocity in on-axis line profiles, ∼1−2 km s^{-1}, yields a mean deprojected speed of $V_{\rm p} \simeq$ 20−40 km s^{-1} for an inclination $i \simeq 87°$ (Claussen et al. 1998). Hence, the outflow cavity is not carved by a fast wide-angle wind at ∼100 km s^{-1}, but by a slower component.

3.2. Comparison with MHD disk wind models

We compared the PV cuts and line profiles with synthetic predictions for steady-state, axisymmetric, self-similar DWs from Keplerian disks, calculated following the equations described in Casse & Ferreira (2000). Two key properties of the MHD solution affect the predictions. First, the magnetic lever arm parameter $\lambda \simeq (r_{\rm A}/r_0)^2$, where $r_{\rm A}$ is the Alfvén radius along the streamline launched from r_0, which determines the extracted angular momentum and poloidal acceleration. Second, the maximum widening $\mathcal{W} = r_{\rm max}/r_0$ reached by the streamline, which controls the flow transverse size. In order to limit the number of free parameters, we kept a fixed inclination $i = 87°$ and stellar mass $M_\star = 0.2\ M_\odot$ (Lee et al. 2017c). The minimum and

[1] http://www.iram.fr/IRAMFR/GILDAS

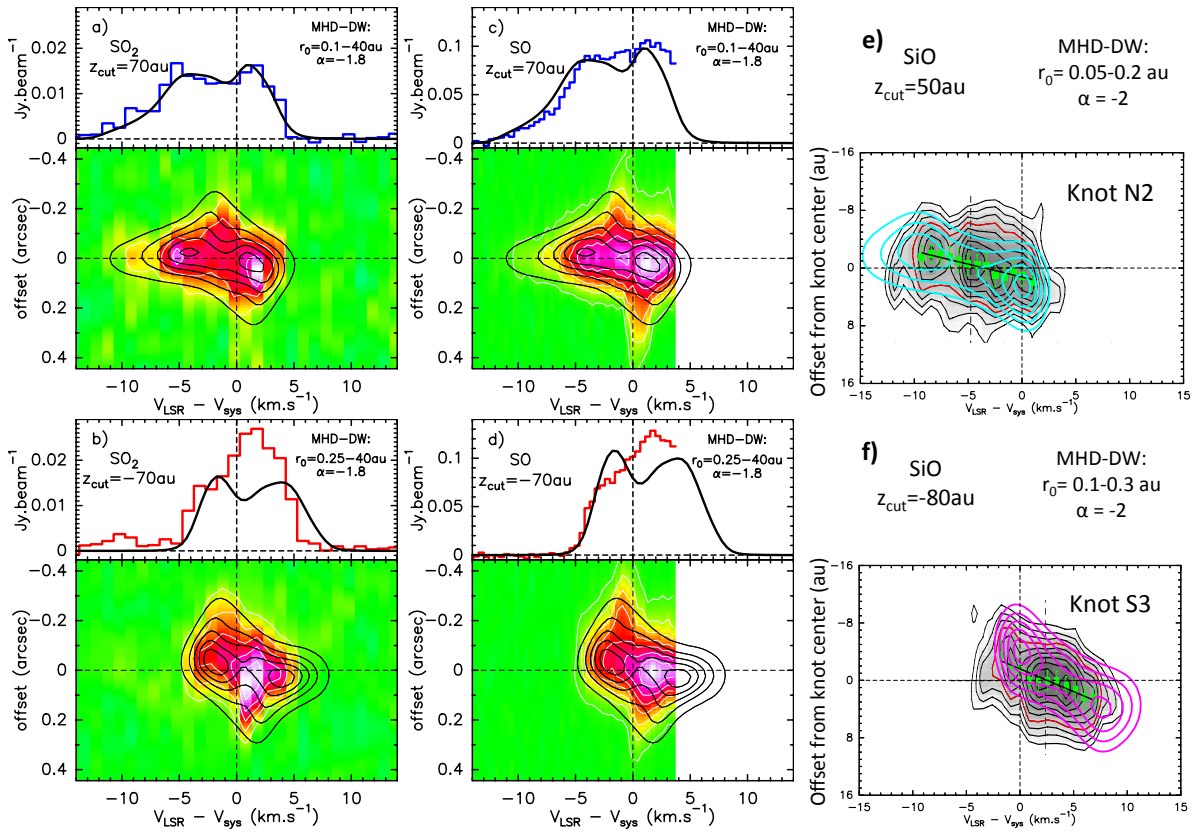

Fig. 2. *Panels a–d*: observed on-axis line profiles (histograms) and transverse PV diagrams (color map and white contours) of SO_2 (*left*) and SO (*middle*) at ±70 au across the northern blue jet (*top*) and the southern red jet (*bottom*). The red wing of SO falls outside our spectral set-up. A DW model fit, with $\lambda = 5.5$ and $\mathcal{W} = 30$ (see text), is overplotted in black for parameters denoted in each panel. *Panels e–f*: PV diagrams observed by Lee et al. (2017a) across the SiO knots N2 and S3 (grayscale and black/red contours). Their measured centroids are shown as green squares and fitted rotation gradient as a black line. The DW model is overplotted in cyan (*top*) or magenta (*bottom*) with parameters denoted above each panel.

maximum launch radii, $r_{\rm in}$ and $r_{\rm out}$, then determine the range of velocities in the wind (through the Keplerian scaling). Since initial SO and SO_2 abundances at the disk surface are very uncertain, we did not compute the emissivity from a full thermo-chemical calculation along flow streamlines, as carried out for H_2O by Yvart et al. (2016). Instead we assumed a power-law variation with radius $\propto r^{\alpha}$ which allowed us to investigate rapidly a broader range of parameters. Synthetic data cubes were then computed assuming optically thin emission and a velocity dispersion of 0.6 km s^{-1} (the sound speed in molecular gas at 100 K), and convolved by a Gaussian beam of the same FWHM as the ALMA clean beam. Parameter α determines the relative weight of inner versus outer streamlines and influences the predicted tilt in the PV. For a given MHD solution, the value of α is well constrained by the slope of the line profile wings.

We find that the DW solution with $\lambda = 13$ used to fit the DG Tau jet in Pesenti et al. (2004) is too fast to reproduce the HH212 data; this solution would require an angle from the sky plane of only 0.5°, outside the observed estimate of $4^{+3^\circ}_{-1^\circ}$ (Claussen et al. 1998). However, we could obtain a good fit for a slower MHD solution with $\lambda = 5.5$ and $\mathcal{W} = 30$. While the emission peaks defining the tilt in PV diagram can be reproduced with $r_{\rm out} = 8$ au, the more extended emission is better reproduced if we increase $r_{\rm out}$ to the expected radius of the Keplerian disk, namely 40 au (Lee et al. 2017c). The corresponding best-fit predictions are superposed in black in Fig. 2. The value of $r_{\rm in}$ is constrained by the highest velocity present in the data; in the blue lobe, the extent of the blue wing suggests $r_{\rm in} \leq 0.1$ au. In the red lobe, our model fit is less good because the centroid is slower than in the blue by a factor 1.5–2. A slower solution with a smaller lever arm (not yet available to us) would probably work better; numerical simulations show that it is indeed possible for a DW to have asymmetric lobes (Fendt & Sheikhnezami 2013). The value $r_{\rm in} \simeq 0.2$ au in Figs. 2b, d is thus only illustrative. The model poloidal speeds at $z = 70$ au range from ∼100 to 2 km s^{-1} for $r_0 = 0.1$ to 40 au.

Interestingly, we find that the same DW solution that fits the SO and SO_2 PV cuts can also reproduce the rotation signatures across axial SiO knots at similar altitude, if SiO traces only inner streamlines launched from 0.05–0.1 au to 0.2–0.3 au. This is shown in Figs. 2e–f, where our synthetic predictions, convolved by 8 au are compared with the ALMA SiO data of Lee et al. (2017a). The predicted range of terminal speeds is 70–170 km s^{-1}, which is consistent with SiO proper motions. Since the dust sublimation radius is also 0.2–0.3 au (Yvart et al. 2016), SiO would be released by dust evaporation at the wind base.

3.3. Biases in analytical estimates of DW outer launch radius

An unexpected result is that our best fitting $r_{\rm out} \simeq 0.2$–0.3 au for SiO knots is 2–10 times larger than the $0.05^{+0.05}_{-0.02}$au estimated by Lee et al. (2017a) with the Anderson et al. (2003) formula, which is valid for all steady DWs. Since the knots are resolved, this cannot be due to beam smearing as in the cases investigated by Pesenti et al. (2004). The same applies to our SO and SO_2 PV cuts, whereas inserting the apparent velocity gradient in the Anderson formula would give $r_{\rm out} \sim 1$ au instead of 40 au.

We explored the reason for this discrepancy and found that the superposition of many flow surfaces along the line of sight creates a shallower velocity gradient leading to strongly underestimate $r_{\rm out}$. A detailed study of this effect, which also leads to underestimating λ, will be presented in Tabone et al. (in prep.).

3.4. Further model tests and limitations

A strong test of the DW picture would be to detect the predicted helical magnetic field structure, for example, through dust polarization measurements with ALMA. Figure 3 plots the poloidal magnetic surfaces in our best-fit model. Beyond the Alfvén surface (at $z/r_0 \simeq 2$), a strong toroidal field develops. In the disk atmosphere at $z \sim 20$ au, brightest in dust continuum, the ratio of toroidal to poloidal magnetic field $B_\phi/B_{\rm p}$ ranges from 1.5 to 10, from outer to inner streamlines. Hence, polarization maps (if not dominated by dust scattering) should not show a pure "hourglass" geometry but be more toroidal closer to the axis.

We also caution that our DW modeling is only illustrative, owing to its simplifications. Notably, self-similarity cannot properly treat the effect of outer truncation. In reality, the shape and dynamics of the last DW streamlines would be determined by pressure balance with the cavity and infalling envelope. As depicted in Fig. 3, they would thus open in the cavity more widely than predicted. This wider opening might explain the broader SO and SO_2 emission beyond the last model contour in PV diagrams and the slow HCO^+ wind noted by Lee et al. (2017c). The opposite pressure effect occurs near the equator, where the thick infalling stream would confine the streamlines inside the CB more tightly than in our model. As shown in Fig. 3, the heating resulting from this interaction might naturally explain the presence of a warm ring of COM emission close to the centrifugal barrier (Lee et al. 2017c; Bianchi et al. 2017). DW models including these effects remain to be developed.

4. Conclusions

Our Cycle 4 ALMA data reveal a rotating wide-angle flow in SO and SO_2 around the SiO jet with a mean speed of ~30 km s^{-1} and an onion-like velocity structure filling in the base of the outflow cavity. Hence, the cavity is not carved by a fast wide-angle wind, but by a slower component. This component emerges from within and up to the centrifugal barrier, and contributes to remove excess angular momentum and mass from this region.

The observed kinematics set tight constraints on stationary, self-similar MHD disk wind models. The lever arm parameter λ should be $\lesssim$5, smaller than in the atomic DG Tau rotating flow (Pesenti et al. 2004), and the launch radii would range from 0.05 to ~40 au, with SiO tracing only dust-free streamlines launched up to 0.2−0.3 au. If such a disk wind is extracting most of the angular momentum required for disk accretion, it would be ejecting 50% of the incoming accretion flow[2]. If this is widespread among low-mass protostars, as suggested by H_2O line profiles (Yvart et al. 2016), this component could strongly contribute to the low core-to-star efficiency $\simeq$30% (e.g. André et al. 2010). We nevertheless caution that our modeling is very idealized and probably not unique. Higher angular resolution and dust polarization maps with ALMA could provide powerful tests of this scenario.

Finally, an important side result of our study is that the apparent rotation gradient strongly underestimates the actual outermost launch radius of an extended MHD disk wind. A detailed study of the magnitude of this effect, which applies beyond HH 212, will be presented in Tabone et al. (in prep.).

[2] $\dot{M}_{\rm ej}/\dot{M}_{\rm acc}(r_{\rm out}) = [1 - (r_{\rm in}/r_{\rm out})^{\xi}]$ with $\xi \simeq 1/(2\lambda - 2)$ when the wind braking torque dominates (Casse & Ferreira 2000).

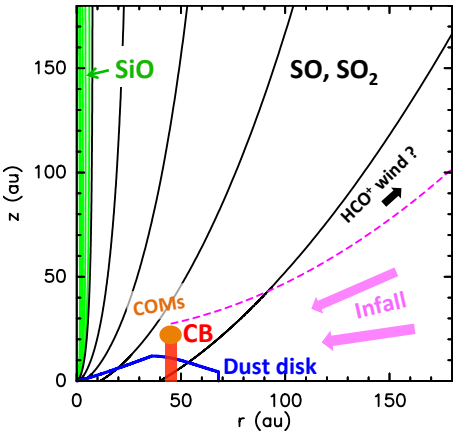

Fig. 3. Schematic view of the inner 180 au of the HH212 system following our MHD disk-wind modeling. The streamlines rich in SiO are pictured in green, the wider component traced by SO and SO_2 is in black, for launch radii of 0.25, 0.9, 3, 11, and 40 au. The magenta dashed curve shows the boundary of the cavity from Fig. 1. The dusty disk scale height from Lee et al. (2017b) is indicated in blue, the centrifugal barrier in red, and the COMs warm ring in orange (Lee et al. 2017c; Bianchi et al. 2017).

Acknowledgements. We are very grateful to K. L. J. Rygl for her support with data reduction at the Bologna ARC node, and we thank the anonymous referee for useful comments. This paper makes use of the ALMA 2016.1.01475.S data (PI: C. Codella). ALMA is a partnership of ESO (representing its member states), NSF (USA), and NINS (Japan), together with NRC (Canada) and NSC and ASIAA (Taiwan), in cooperation with the Republic of Chile. The Joint ALMA Observatory is operated by ESO, AUI/NRAO, and NAOJ. This work was supported by the Programme National "Physique et Chimie du Milieu Interstellaire" (PCMI) of CNRS/INSU with INC/INP and co-funded by CNES, and by the Conseil Scientifique of Observatoire de Paris. This research has made use of NASA's Astrophysics Data System.

References

Anderson, J. M., Li, Z.-Y., Krasnopolsky, R., & Blandford, R. D. 2003, ApJ, 590, L107
André, P., Men'shchikov, A., Bontemps, S., et al. 2010, A&A, 518, L102
Bacciotti, F., Ray, T. P., Mundt, R., Eislöffel, J., & Solf, J. 2002, ApJ, 576, 222
Béthune, W., Lesur, G., & Ferreira, J. 2017, A&A, 600, A75
Bianchi, E., Codella, C., Ceccarelli, C., et al. 2017, A&A, 606, L7
Bjerkeli, P., van der Wiel, M. H. D., Harsono, D., Ramsey, J. P., & Jørgensen, J. K. 2016, Nature, 540, 406
Casse, F., & Ferreira, J. 2000, A&A, 353, 1115
Claussen, M. J., Marvel, K. B., Wootten, A., & Wilking, B. A. 1998, ApJ, 507, L79
Codella, C., Cabrit, S., Gueth, F., et al. 2014, A&A, 568, L5
Fendt, C., & Sheikhnezami, S. 2013, ApJ, 774, 12
Ferreira, J., Dougados, C., & Cabrit, S. 2006, A&A, 453, 785
Hirota, T., Machida, M. N., Matsushita, Y., et al. 2017, Nature Astronomy, 1, 0146
Launhardt, R., Pavlyuchenkov, Y., Gueth, F., et al. 2009, A&A, 494, 147
Lee, C.-F., Hirano, N., Zhang, Q., et al. 2014, ApJ, 786, 114
Lee, C.-F., Ho, P. T. P., Li, Z.-Y., et al. 2017a, Nature Astronomy, 1, 0152
Lee, C.-F., Li, Z.-Y., Ho, P. T. P., et al. 2017b, Sci. Adv., 3, e1602935
Lee, C.-F., Li, Z.-Y., Ho, P. T. P., et al. 2017c, ApJ, 843, 27
Louvet, F., Dougados, C., Cabrit, S., et al. 2016, A&A, 596, A88
Matthews, L. D., Greenhill, L. J., Goddi, C., et al. 2010, ApJ, 708, 80
Panoglou, D., Cabrit, S., Pineau Des Forêts, G., et al. 2012, A&A, 538, A2
Pesenti, N., Dougados, C., Cabrit, S., et al. 2004, A&A, 416, L9
Podio, L., Codella, C., Gueth, F., et al. 2015, A&A, 581, A85
Yvart, W., Cabrit, S., Pineau des Forêts, G., & Ferreira, J. 2016, A&A, 585, A74
Zhu, Z., & Stone, J. M. 2017, ArXiv e-prints [arXiv:1701.04627]

Appendix A: SO and SO_2 channel maps

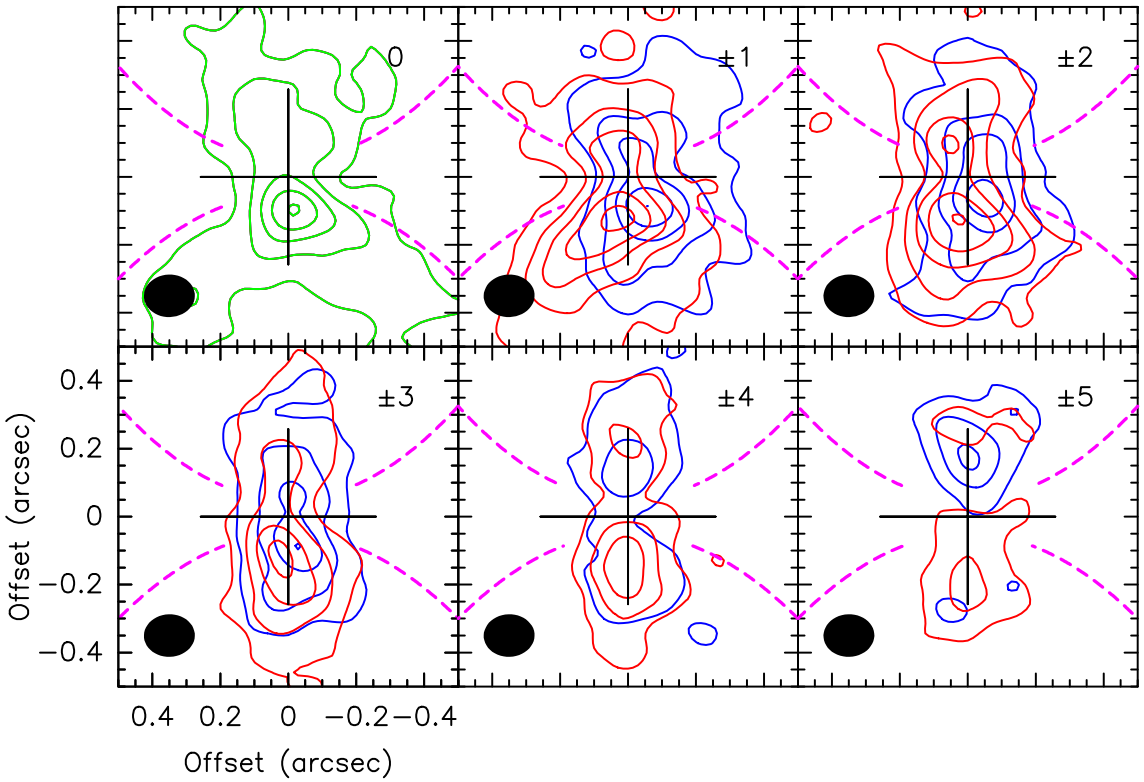

Fig. A.1. Channel maps of continuum-subtracted SO_2 $8(2,6) - 7(1,7)$ emission within ±0.5″ of the central source of HH212. The velocity offset from the systemic velocity (V_{sys} = 1.7 km s^{-1}) is indicated (in km s^{-1}) in the upper right corner with blue and red contours denoting blueshifted and redshifted emission. The channel width is 1 km s^{-1}. First contour and steps corresponds to 4σ and 6σ (σ = 1 mJy/beam), respectively. The $C^{34}S$ cavity boundary from Fig. 1 is drawn in magenta dashed lines.

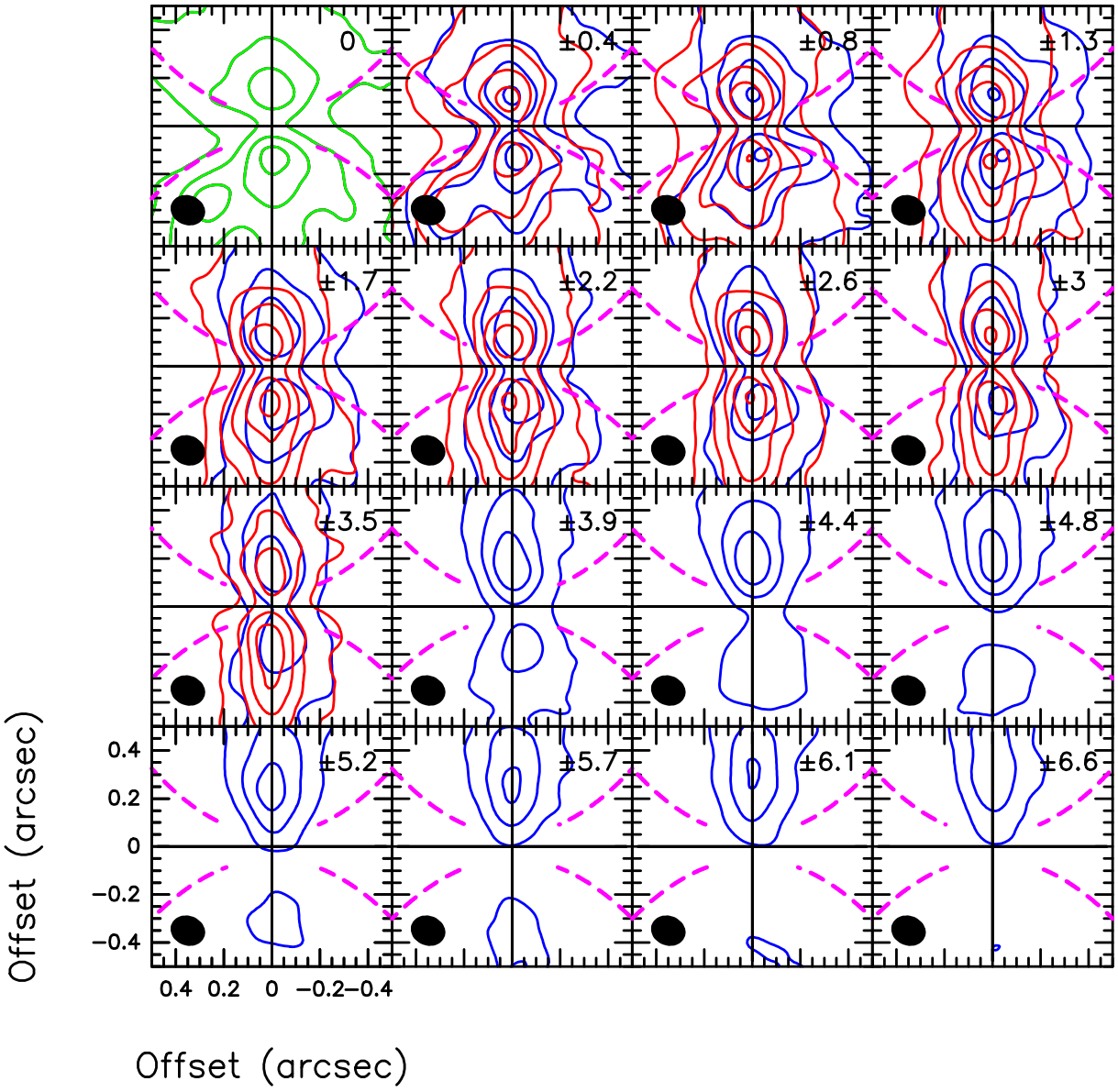

Fig. A.2. Channel maps of continuum-subtracted SO 9_8-8_7 emission within ±0.5″ of the central source of HH212. The velocity offset from the systemic velocity (V_{sys} = 1.7 km s^{-1}) is indicated (in km s^{-1}) in the upper right corner with blue and red contours denoting blueshifted and redshifted emission. The channel width is 0.44 km s^{-1}. First contour and steps corresponds to 6σ and 16σ (σ =1.7mJy/beam), respectively. The C^{34}S cavity boundary from Fig. 1 is drawn in magenta dashed lines.